Preprint submitted to International Journal of Thermal Sciences
https://doi.org/10.1016/j.ijthermalsci.2018.07.044

Experimental study of the effectiveness of air curtains of variable width and injection angle to block fire-induced smoke in a tunnel configuration

Long-Xing Yu[1,2]; Fang Liu[1]; Tarek Beji[2]; Miao-Cheng Weng[1*]; Bart Merci[2]*

[1]Chongqing University, Faculty of Urban Construction and Environmental Engineering, Chongqing, China

[2]Ghent University – UGent, Dept. of Flow, Heat and Combustion Mechanics, Ghent, Belgium

**Corresponding author*

Fang Liu: drliufang@126.com, Chongqing University, Shapingba District, 400045, P.R. China

Miao-Cheng Weng: mcweng@outlook.com, Chongqing University, Shapingba District, 400045, P.R. China

Abstract

Small-scale experiments have been conducted to study the sealing effect of an air curtain for fire-induced smoke confinement in a tunnel configuration. The processed data confirmed the results obtained earlier from blind Computational Fluid Dynamics (CFD) simulations [1] using the Fire Dynamics Simulator (FDS) 6.5.3 [2, 3]. Furthermore, the CFD simulations provided complementary information on the detailed flow and temperature fields which are difficult to obtain in experiments with the available techniques. A parametric study is performed, covering a range of air curtain velocities, slot widths, injection angles and total fire heat release rates (HRRs). The momentum ratio R, defined as the ratio of the vertically downward air curtain momentum to the horizontal smoke layer momentum at the position of the air curtain, is confirmed to be a key parameter for the air curtain performance. A ratio R ≈ 10 is recommended for the optimum sealing effect in terms of smoke confinement. In addition, two other important parameters that determine the performance of air curtains for smoke confinement are presented. The first parameter is the dimensionless

shape factor AR (AR=Width/Length) that characterizes the dilution effect of the air curtain jet. The second parameter is the injection angle θ that characterizes the horizontal force of the air curtain. The air curtain sealing effectiveness increases with both the increase of slot width (shape factor AR) and injection angle (θ). The air curtain width has a limited influence on the performance of the air curtain whilst the injection angle has a more significant influence on the sealing effectiveness of the air curtain for the scenarios considered in this study. An optimal injection angle of 30^{o} inclined to the fire source is recommended in the engineering design of the air curtain for smoke confinement for situations where the fire location can be pre-determined to be only at one side of an air curtain.

Key words: Smoke confinement; Air curtain; Tunnel fire; Experiment; FDS.

1. Introduction

It is well-known that smoke is the most fatal factor in fires, and about 85% of people killed in building fires were killed by toxic smoke [4, 5]. Smoke and heat control systems are an essential part of fire protection in the fire safety design of buildings. In the event of a fire, the air curtains (in various building configurations) have been proven to be effective in smoke confinement. The main advantage of such virtual screens, compared to the traditional fire doors, is the easy evacuation of people while still limiting smoke and heat transfer through the opening [6].

Air curtains based on the push-pull system have been shown to be effective in preventing suffocation caused by smoke during evacuation in a corridor [7]. Hu

et al. [8] also reported, by means of small-scale experiments and numerical simulations obtained with the code Fire Dynamics Simulator (FDS, Version 4.0.7), that the single-jet air curtain can be an effective way for smoke and CO confinement in channel fires. Also the Computational Fluid Dynamics (CFD) code FLUENT has been used for investigating air curtain flows numerically. Ji et al. [9] carried out a theoretical analysis and FLUENT simulations of smoke control by means of an air curtain in long channels and developed formulas providing the critical conditions to prevent smoke from intruding the protected side. Krajewski and Węgrzyński [10] studied the use of air curtains in fire safety as a barrier for heat and smoke by means of bench experiments and FLUENT (version 13.0). Again, they confirmed the potential use of air curtains as a tool for fire safety in buildings. Their work also shows the possibilities of CFD (Ansys Fluent) in designing air curtains used in fire safety engineering. The capabilities of FDS was also studied in [11, 12]. In addition, the influence of various parameters on the performance of an air curtain is reported in [10]. However, the result is based on the assumption that the only important destabilizing factor for the air curtain is the uniform pressure difference. Besides tunnel and corridor-like configurations, air curtains were installed and tested at the entrance of a stairwell [13] and an evacuation passageway [14].

In a nutshell, all the studies mentioned above indicate that air curtains can be useful for confinement of smoke during a fire. Nevertheless, to the best of our knowledge, the only real case where an air curtain has been actually installed is in a road tunnel called the A86 West Underground Link-up of Paris, in France [15]. However, there is no data indicating how such systems should be designed [16] to optimize their efficiency. For example, there is a lack of

information on the appropriate jet properties in terms of discharge velocity, injection angle and slot width. Therefore, it is of great important to study the sealing effectiveness and the main parameters that affect the performance of air curtains for smoke blocking.

It is interesting though to note that there have been studies on the design of air curtains in various applications such as energy savings [17], comfort ventilation [18] and air pollution control [19], but none of them is intended to stop smoke spread in the event of a fire. The air curtain design method discussed in [20, 21] and based on the free jet theory under the assumption of uniform transversal pressure difference is not suitable for a fire.

In the specific context of a fire, the transverse force of the ceiling jet destabilizing the air curtain is much stronger than the natural convection flow in the other applications. In fact, in the numerical study carried out in [1] by means of CFD, the sealing effect (i.e., propensity to block smoke spread) of an air curtain in a tunnel configuration is found to be dependent on the ratio, R, of the vertically downward air curtain momentum to the horizontal smoke layer momentum at the position of the air curtain. More specifically, the maximum sealing effectiveness is obtained for values of R between 8 and 10 [1].

The simulations carried out in [1] were blind in that no experimental data were available to confirm the validity of the results. In the present work, we present data from 90 small-scale experimental tests with complementary information obtained from CFD (more specifically, FDS [22]) on the detailed flow field in order to characterize the ceiling jet. Moreover, we focus on the specific effects of the air curtain width and injection angle, which has not been discussed before.

2. Experimental set-up

Reduced-scale experiments have been carried out to examine the influence of the jet properties on the sealing effect of the air curtain. Details of the experiments are described hereafter, including the experimental apparatus, fire source and air curtain set-up, instrumentation, experimental schemes and procedure and data processing.

2.1 The experimental apparatus

Figure 1 shows the reduced-scale model (3.00 m long, 0.32 m wide and 0.48 m high) used in this work. The model simulated a fire within a ‘corridor-like’ (or ‘tunnel-like’) compartment and the smoke propagating along the evacuation passageway. The entry and exit of the ‘tunnel-like’ enclosure are open to the outside. An air curtain was installed at the ceiling (see Fig.1) to block smoke spread to the downstream region. The tunnel (floor, ceiling and the frame) was constructed from 1.25 mm thick stainless steel. For visualization, the front and back faces of the tunnel were constructed from 5 mm thick anti-fire glass.

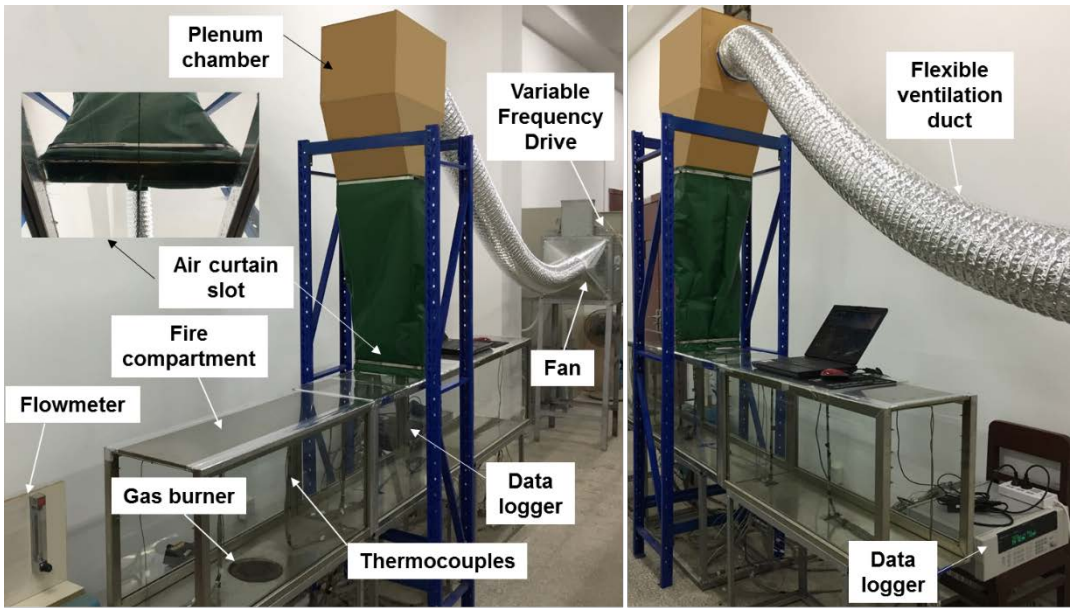

Figure 1. *Photo of the test section and the instrumentation before testing.*

2.2 The fire source

A Liquefied Petroleum Gas (LPG) gas burner with active flow control was employed to model a burning object. The diameter of the fire source is 16 cm with small nozzles scattered on the fire surface. The fire source is located on the floor at 0.5 m away from the left opening of the fire compartment. Details of the positions are shown in section 2.4. The main advantage of using a gas burner is the easily controllable heat release rate, via a fuel flow controller. The total heat release rate ($\dot{Q}$) of the fire was determined from the heat of combustion (per unit volume) of the fuel (ΔH_c) and the volume flow rate of the fuel ($\dot{V}$), assuming a combustion efficiency (χ) of 100% [23-25]:

$$\dot{Q} = \chi \cdot \Delta H_c \cdot \dot{V} \quad (1)$$

The heat of combustion of LPG (57.55 MJ/m^3) was measured by the water flow calorimeter. Two fires with HRRs of 3.62 kW and 2.92 kW were considered. Based on Froude scaling ($\dot{Q}_m/\dot{Q}_f = (L_m/L_f)^{5/2} = {\lambda_L}^{5/2}$, where the subscripts *m* and *f* respresent respectively the reduced-scale model and the full scale and *L* is a representative dimension of the set-up) the corresponding full-scale HRRs are 3.2 MW and 2.5 MW, considering a geometrical scale-up factor of 15. Figure 2 shows the porous gas burner (household type) and LPG flames used in this work.

Figure 2. *Porous gas burner and LPG flame, 3.62 kW (left) and 2.92 kW (right).*

2.3 The air curtain

As shown in Figure 1, an axial fan was used to supply the air. The fan speed was controlled by the velocity controller (variable frequency drive, VFD). A plenum chamber was used to equalise the pressure for a more even distribution of velocity at the air curtain outlet.

Different air curtain slots were constructed beforehand in order to be tested in the experiments. Three air curtain widths (W=1 cm, 2 cm and 3 cm) were considered. A zoom-in photo of air curtain slot used in the experiment is shown in Fig.1.

The air curtain velocities at different setting numbers of velocity controller (variable frequency drive, VFD), e.g., at 10, 20, 30, 40, 50 Hz, were measured by anemometer sensors (SWA 03+, omnidirectional probes) before the experiment. Four positions (at 1/5, 2/5, 3/5 and 4/5) across the length of the air curtain (in the centreline of the outlet) were measured. The measurement was repeated twice for each test. An average value was used as the maximal mean velocity of the air curtain along the centreline of the outlet. The velocity data is presented in Table 1.

Figure 3 displays the variation of the air curtain momentum ($\rho_j A_j V_j^2$) and mass flow rate ($\rho_j A_j V_j$) with different slot widths as a function of the fan frequency for several fire HRRs and slot widths. The air density (ρ_j) is calculated based on the measured ambient temperature of each test shown in Table 1. The average velocity of the air curtain slot (V_j) is calculated based on the measured maximum velocity at the center and the power-law velocity profile [26] for fully turbulent flow from a slot.

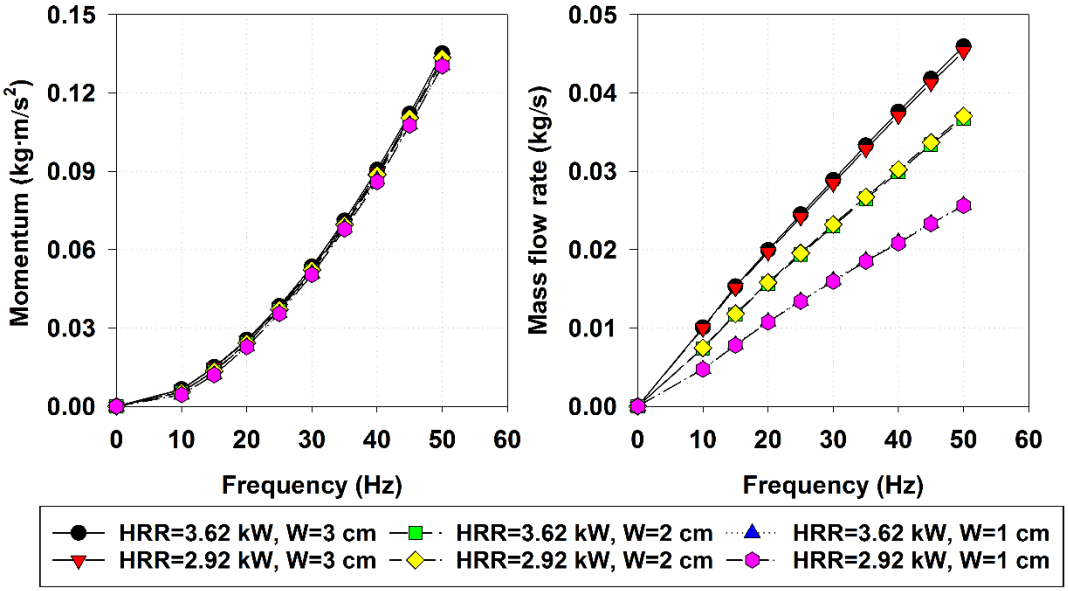

Figure 3. *Air curtain momentum (left) and mass flow rate (right) as a function of the fan frequency.*

The results displayed in Fig.3, on the left, show that the air curtain momentum varies only with the fan frequency (and thus the fan power). For a fixed frequency, there is no variation in momentum with the HRR or the slot width, which confirms the accuracy and repeatability of the measured velocity data.

The results displayed in Fig.4, on the right, show that, for a fixed fan frequency (and thus fixed momentum), the mass flow rate decreases as the slot width decreases. This effect will be discussed in more detail in section 4.

2.4 Instrumentation

The main quantity recorded for the present experiment is the gas temperature. The temperature measuring system consists of 87 thermocouples and a data logging system. The thermocouples were arranged to measure both the longitudinal smoke temperature distribution along the test section and the vertical temperature distribution of the smoke layer. In order to better capture the temperature gradients close to the boundaries, more thermocouples were positioned near the ceiling and floor (with a narrow spacing) along the height of the tunnel.

K-type bare-bead thermocouples (Nickel-Chromium/Nickel-silicon) with a diameter of 0.5 mm, a response time of less than 1 second and a measurement error less than 3% were used. All the thermocouples were connected to a data logging system with the data recorded every 5 seconds (the pace of a scan sweep). Figure 4 shows the details of the thermocouple locations and spacing.

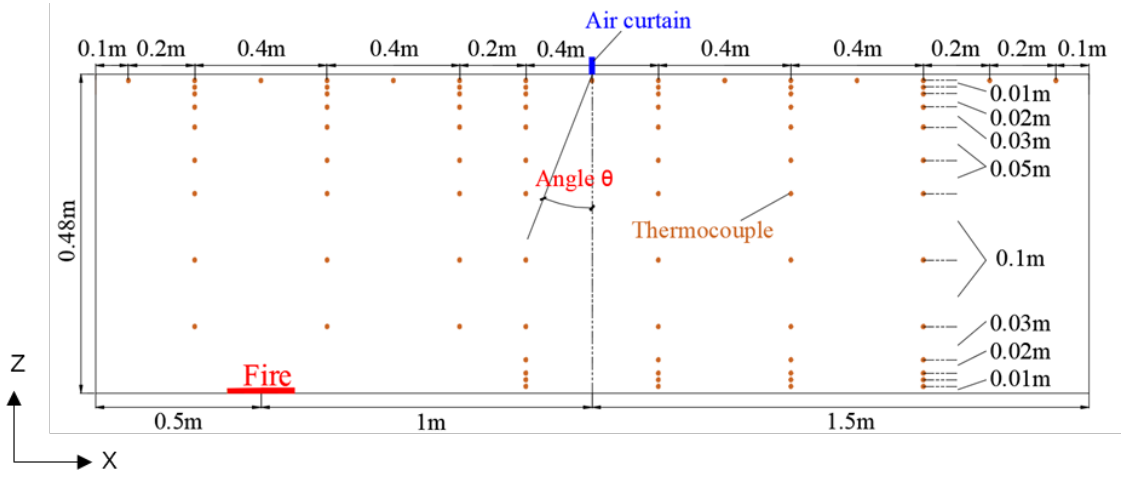

Figure 4. *Sketch of thermocouple positions (Not drawn to scale)*

2.5 Experimental schemes and procedure

The parameters of interest which may affect the sealing effect of the air curtain

are the fire HRRs, jet discharge velocity, slot width and injection angle of the plane jet. First, 2 fire HRRs (3.62 kW and 2.92 kW) and 10 jet discharge velocities (0-7.72 m/s) for each of the 3 air curtain slots (W=1 cm, 2 cm and 3 cm) will be examined for a vertical-downward air curtain (i.e., injection angle θ=0°, see Fig. 4). After that, 3 other injection angles of the plane jet (θ=15°, 30°, 45°) will be studied at 10 jet discharge velocities (0-7.72 m/s), 1 air curtain slot width (W=3 cm) and 1 fire HRR (3.62 kW). Thus, in total, 90 experiments were carried out. The series of experiments are shown in Table 1 (a) and (b).

The experimental procedure was as follows:

1) Start the data recording system for 30 s to record the ambient temperature;

2) At 30 s, turn on the fire at pre-setting value of HRR immediately;

3) At 240 s, turn on the air curtain at the pre-setting value of velocity immediately;

4) At 660 s, first stop the fire, then at 780 s stop the air curtain, at 900 s stop the recording system.

5) Start the next experiment after the fire compartment cooled down sufficiently to the ambient temperature. Repeat 1-5.

Table 1 (a). Overview of experimental tests for a vertical-downward air curtain.

Test	Slot width (cm)	HRR (kW)	Air curtain velocity (m/s)	Ambient Temp. (°C)	Air curtain momentum (10^{-3} kg m/s^2)	Ceiling jet momentum (10^{-3} kg m/s^2)	Ratio (R)
1	3	3.62	0.00	24.21	0.00	5.64	0.00
2			0.98	23.93	6.50		1.15
3			1.49	24.09	15.03		2.67
4			1.94	24.13	25.47		4.52

5			2.38	23.69	38.39		6.81
6			2.81	23.96	53.46		9.48
7			3.24	23.97	71.07		12.61
8			3.66	24.14	90.64		16.08
9			4.07	24.27	112.04		19.87
10			4.47	24.15	135.20		23.98
11		2.92	0.00	27.77	0.00	5.04	0.00
12			0.98	28.21	6.41		1.27
13			1.49	28.29	14.82		2.94
14			1.94	28.28	25.12		4.99
15			2.38	28.06	37.83		7.51
16			2.81	28.51	52.66		10.46
17			3.24	28.27	70.06		13.91
18			3.66	28.38	89.37		17.75
19			4.07	28.10	110.62		21.97
20			4.47	28.20	133.38		26.49
21	2	3.62	0.00	29.90	0.00	5.64	0.00
22			1.10	29.96	5.35		0.95
23			1.74	29.88	13.40		2.38
24			2.33	29.78	24.03		4.26
25			2.88	29.98	36.70		6.51
26			3.42	30.04	51.74		9.18
27			3.95	30.40	68.93		12.23
28			4.46	30.36	87.89		15.59
29			4.98	30.26	109.62		19.44
30			5.47	30.40	132.19		23.45
31		2.92	0.00	27.58	0.00	5.04	0.00
32			1.10	27.02	5.41		1.07
33			1.74	26.84	13.53		2.69
34			2.33	27.10	24.25		4.82
35			2.88	27.04	37.06		7.36
36			3.42	27.08	52.25		10.37
37			3.95	27.82	69.52		13.81
38			4.46	27.45	88.74		17.62
39			4.98	27.94	110.46		21.94
40			5.47	27.51	133.46		26.50
41	1	3.62	0.00	30.23	0.00	5.64	0.00
42			1.42	30.11	4.44		0.79
43			2.34	29.79	12.16		2.16
44			3.22	30.11	22.95		4.07
45			4.03	31.46	35.69		6.33
46			4.80	30.95	50.86		9.02
47			5.57	31.05	68.30		12.12
48			6.27	31.11	86.75		15.39
49			7.02	32.76	107.98		19.15
50			7.72	32.89	130.64		23.17
51		2.92	0.00	31.74	0.00	5.04	0.00

52			1.42	31.92	4.41		0.88
53			2.34	32.96	12.04		2.39
54			3.22	32.38	22.78		4.52
55			4.03	33.24	35.48		7.05
56			4.80	33.57	50.43		10.01
57			5.57	33.30	67.80		13.46
58			6.27	33.71	86.02		17.08
59			7.02	33.76	107.62		21.37
60			7.72	33.69	130.30		25.87
Note: the ceiling jet momentum is calculated from FDS and the momentum ratio R is calculated as air curtain momentum divided by ceiling jet momentum (See section 4.1). Injection angle θ=0°.							

Table 1 (b). Overview of experimental tests for non-vertical-downward air curtains.

Test	Injection angle	Air curtain velocity (m/s)	Ambient Temp. (°C)	Air curtain momentum (10^{-3} kg m/s^2)	Ceiling jet momentum (10^{-3} kg m/s^2)	Ratio (R)
61	15°	0.00	27.90	0.00	5.64	0.00
62		0.98	27.75	6.42		1.14
63		1.49	28.28	14.82		2.63
64		1.94	27.93	25.15		4.46
65		2.38	28.34	37.79		6.70
66		2.81	27.92	52.76		9.36
67		3.24	28.07	70.11		12.43
68		3.66	27.73	89.56		15.89
69		4.07	27.16	110.96		19.68
70		4.47	27.35	133.76		23.72
71	30°	0.00	26.55	0.00	5.64	0.00
72		0.98	26.34	6.45		1.14
73		1.49	26.67	14.90		2.64
74		1.94	26.80	25.24		4.48
75		2.38	26.73	38.00		6.74
76		2.81	27.59	52.82		9.37
77		3.24	26.90	70.38		12.48
78		3.66	27.32	89.68		15.91
79		4.07	26.88	111.07		19.70
80		4.47	27.01	133.91		23.75
81	45°	0.00	25.86	0.00	5.64	0.00
82		0.98	25.93	6.46		1.15
83		1.49	26.22	14.92		2.65
84		1.94	26.06	25.30		4.49
85		2.38	26.02	38.09		6.76
86		2.81	25.71	53.15		9.43

87		3.24	26.01	70.59		12.52
88		3.66	25.97	90.09		15.98
89		4.07	26.03	111.38		19.76
90		4.47	25.78	134.46		23.85
Note: W=3 cm and fire HRR=3.62 kW.						

2.6 Data processing

In all experiments, a period of 15 mins (900 s) in total is covered. Both the temporal evolution and the time-averaged values of the recorded data will be analyzed. For obvious reasons, the flow field experienced strong fluctuations with the air curtain in operation. Nevertheless, a (quasi) steady-state situation [27] can be considered during the period of 600-660s over which time-averaged values have been calculated for all the tests.

Figure 5 shows the temporal evolution of temperature at 1cm below the ceiling at selected positions in different tests. Test 1 (Top: in the absence of air curtain) and Test 5 (Bottom: with activation of air curtain) are selected as representative profiles. The solid-black line (ΔX=0 m) shows the temperature of the thermocouple above the fire source. The dashed-green line (ΔX=1 m) shows the temperature of the thermocouple below the air curtain slot. The dotted-red line (ΔX=0.8 m) and the dash-dot-blue line (ΔX=1.2 m) show the temperature of the thermocouple at the symmetric positions upstream and downstream the air curtain.

A fast increase of temperature was observed when the fire was ignited at 30 s. Then the temperature increased slowly to a plateau at around 600 s (seeing the temperature curves approaching a horizontal asymptote) for Test 1. For Test 5, a clear decrease of temperature in the downstream region was observed when the air curtain was activated at 240 s. To be noted, a decrease of temperature above the fire source was also observed. This is due to the stronger back-flow

with fresh air moving to the fire source as the air curtain velocity increases. When the fire was turned off at 660 s, the temperature at the upstream of the air curtain drops suddenly. At 780 s, after stopping the air curtain, the temperature below the air curtain increases slightly. The evolution of the temperature fully reflects the experimental procedure aforementioned.

In the absence of an air curtain, the flow field reached a (quasi) steady-state from 600-700 s onwards. With the activation of the air curtain, the flow field generally reached the (quasi) steady-state faster, at around 400 s. To simplify the data processing, all the mean values processed in the experiments by averaging the results over the period of 600-660s.

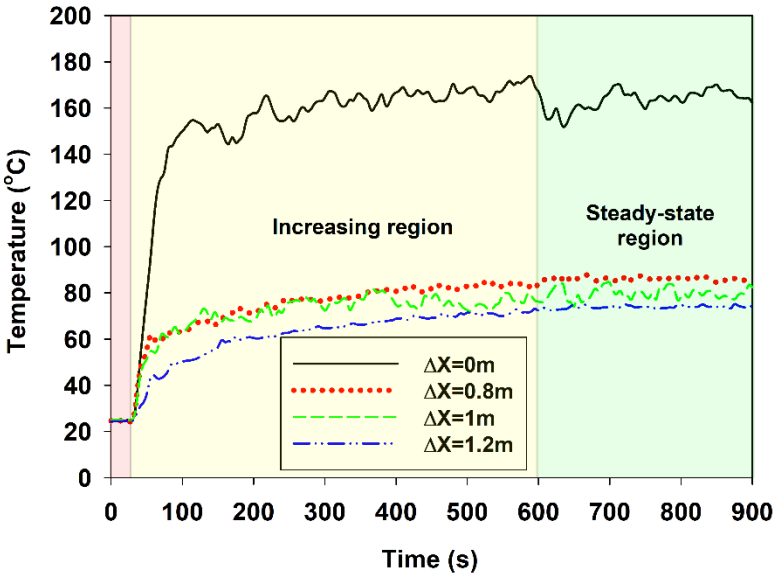

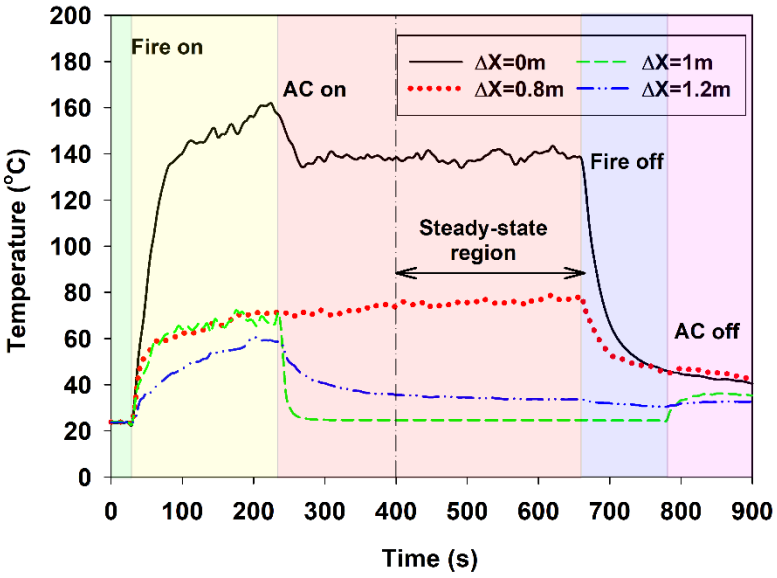

Figure 5. *Temporal evolution of temperature at selected positions in different experiments. Top (Test 1), Bottom (Test 5)*

3. Characterization of the ceiling jet momentum using CFD

As shown in [1], the sealing effect of an air curtain depends on the ratio R of the vertically downward air curtain momentum to the horizontal smoke layer (i.e., ceiling jet) momentum at the position of the air curtain. In order to estimate the latter, ceiling jet velocities must be measured. Unfortunately, this was not possible with the available hot-wire anemometer technique. Therefore, numerical simulations have been carried out with FDS for tests 1, 11, 21, 31, 41 and 51 where no air curtain was activated. The accuracy of these simulations will be assessed by comparing the predicted and measured temperature for the 87 positions displayed in Fig.4. After validation, the numerical results will be used to estimate the ceiling jet (1) thickness, (2) average velocity and (3) average density (from the temperature field and the ideal gas law), which are the three parameters required to calculate the ceiling jet momentum.

3.1 Setup of the numerical simulations

3.1.1 Geometry and boundary conditions

Numerical simulations of the experimental tests have been carried out, keeping the same dimensions of the fire compartment.

The left and right end of the fire compartment are set open to the outside by specifying the 'OPEN' boundary condition in FDS. The four other sides are 'solid' boundary conditions. Detailed solid material properties are shown in Table 2.

Table 2. Summary of solid material properties.

Material	Thickness (m)	Specific heat (kJ/kg·k)	Conductivity (W/m·k)	Density (kg/m^3)	Emissivity
Stainless steel	0.00125	0.46	45.8	7850	0.074
Glass	0.005	0.84	0.76	2700	0.92

The fire source boundary condition has been set by prescribing a heat release rate per unit area (HRRPUA) over a 0.0172 m^2 round solid surface flush with the floor (which was set up using the stair stepping method, since Cartesian coordinates are used in FDS). The prescribed values of the HRRPUA were 210 and 170 kW/m^2, which corresponds to, respectively, 3.62 and 2.92 kW.

A sensitivity study (not shown here) on the radiative fraction of the fire indicates that the default FDS value of 30% is appropriate for LPG burning. According to the measurements of Tewarson [28], the radiative fractions of propane (C_3H_8) and Butane (C_4H_{10}) are respectively 28.6 % and 30.5%. For LPG, made of 35% propane and 65% butane [29], the radiative fraction of LPG is calculated as 30%, which again confirms the validity of applying a radiative fraction of 30% for the simulated fire in FDS.

3.1.2 Grid resolution and turbulence modelling

Uniform cubic cells are used in all simulations. Four grid resolutions have been tested, i.e., 2, 1, 0.8 and 0.5 cm, resulting in a grid of respectively 57600, 460800, 900000 and 3686400 cells.

In FDS, turbulence is modeled within the Large-Eddy Simulations (LES) framework. The dynamic Smagorinsky turbulence model has been applied in all the simulations because, in this case, no tuning is required for the model parameter C_s used in the calculation of the sub-grid scale viscosity. Details on the influence of turbulence model have been discussed in a previous study [30].

3.2 Validation of the FDS simulations

The overall uncertainty of the numerical simulations for the temperature prediction at the level of the 87 positions displayed in Fig.4 has been estimated based on the methodology developed in [31]. In this methodology, the model uncertainty is calculated based on all the measured values, corresponding predicted values and the experimental uncertainty (taken here to be 5%). The simulations of test 1 with cell sizes of 2, 1, 0.8 and 0.5 cm resulted in a model uncertainty of respectively 13.3, 6.4, 5.0 and 5.3 %. Therefore, a cell size of 0.8 cm is deemed adequate to examine the fire induced flow. Note also that this grid resolution satisfied the suggested criterion of having at least 10 cells fitting within the dimensionless diameter D* [32].

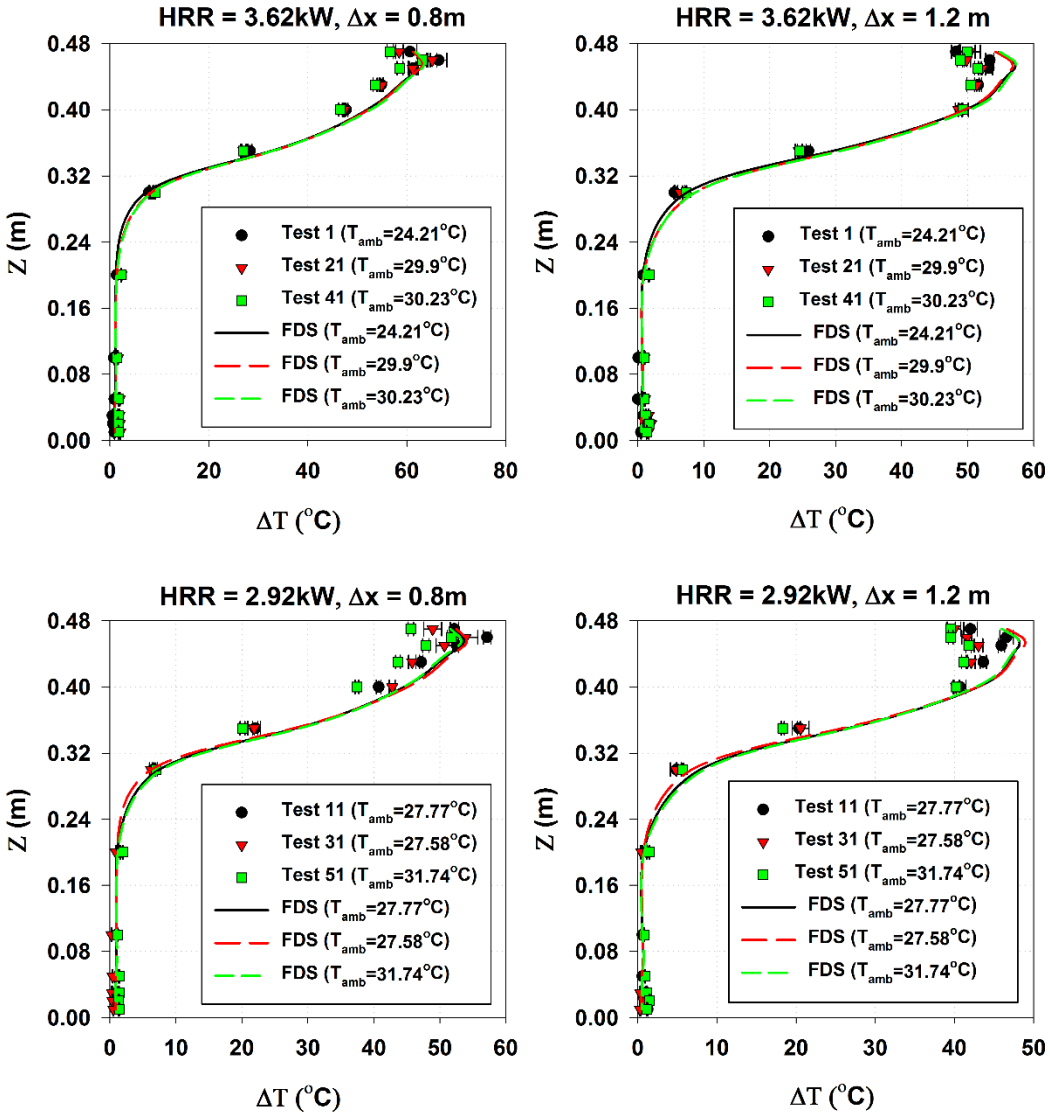

Figure 6. *Comparisons of experimental data to FDS results on the time averaged smoke temperature distribution across different sections. Top: HRR=3.62 kW (Test 1, 21 & 41); Bottom: HRR=2.92 kW (Test 11, 31 & 51).*

In addition to the overall deviation between model predictions and experimental data, the time averaged smoke temperature distributions across different sections have been examined. The results displayed in Fig.6 show a good agreement, which confirms the quality of the simulations and justifies the use of the numerical predictions to characterize the ceiling jet.

3.3 Characterization of the ceiling jet momentum

Figure 7 shows the time averaged velocity profiles in the smoke layer at the air curtain position (ΔX = 1 m) for different fire HRRs at different ambient temperatures, in the absence of an air curtain. As expected, the horizontal velocity of the smoke layer increases as the fire HRR increases. This is due to the increased energy injection and the increased buoyancy, enhancing the entrainment into the vertically rising smoke plume and thus adding to the horizontal momentum of the smoke layer underneath the ceiling. The influence of ambient temperature is minor.

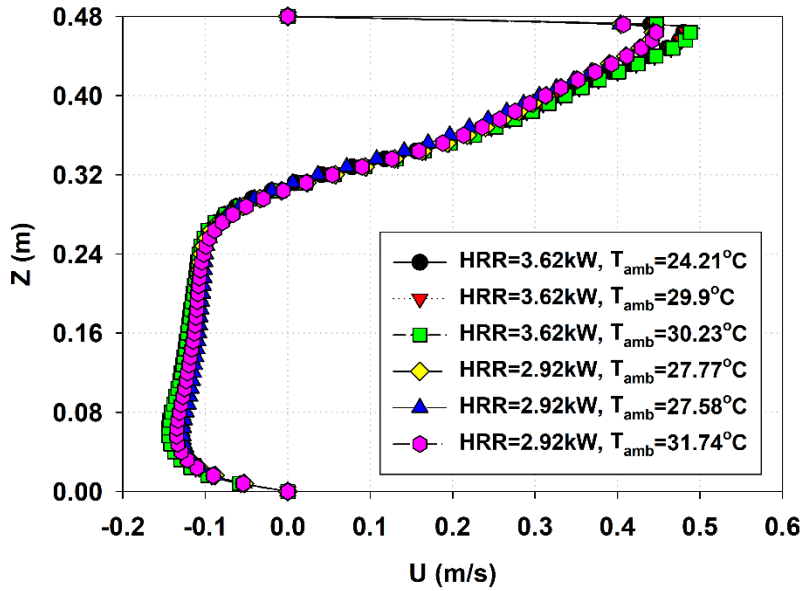

Figure 7. *FDS results on time averaged velocity profiles in the smoke layer at the air curtain position (ΔX = 1 m) for different fire HRRs at different ambient temperatures.*

The velocity profiles displayed in Fig.7 are first used to determine the ceiling jet depth which spans from the ceiling up to the height where the horizontal velocity is null. Then, the ceiling jet momentum is calculated as an integration across the ceiling jet depth times the ceiling jet width (equal to the length of the air curtain L = *0.32 m*):

$$\rho_s A_s V_s^{\,2} = L \cdot \int \rho_s v_s^{\,2} dz \quad (2)$$

The outcome of this procedure is displayed in Table 3 for tests 1, 11, 21, 31, 41 and 51. An average value of the data obtained in Table 3 is embedded in Table 1.

Table 3. Ceiling jet properties determined from CFD.

Test	1	11	21	31	41	51
Depth (m)	0.168	0.168	0.168	0.168	0.168	0.168
Momentum (10^{-3} kg m/s^2)	5.54	5.64	5.73	5.06	5.05	5.00

4. Results and discussion

4.1 General observations

4.1.1 Influence of the air curtain velocity

Figure 8 shows the mean smoke temperature distribution along the longitudinal direction at 1 cm below the ceiling (Test 1-10: HRR=3.62 kW and W=3 cm). It shows that without the activation of an air curtain (0 m/s), as shown in many previous researches [33, 34], the smoke layer temperature decreases gradually with increasing distance from the fire source. With the activation of the air curtain, the temperature behind the air curtain at the same position was reduced compared to the case without the activation of the air curtain. The reduction of temperature becomes stronger as the air curtain velocity increases. However, velocities of around 2 m/s or higher show very similar results in the downstream region. This may be due to the counterbalance effect of increased blocking effect by the air curtain and stronger impinging jet onto the floor, pushing more smoke into the downstream region, as the momentum ratio R increases.

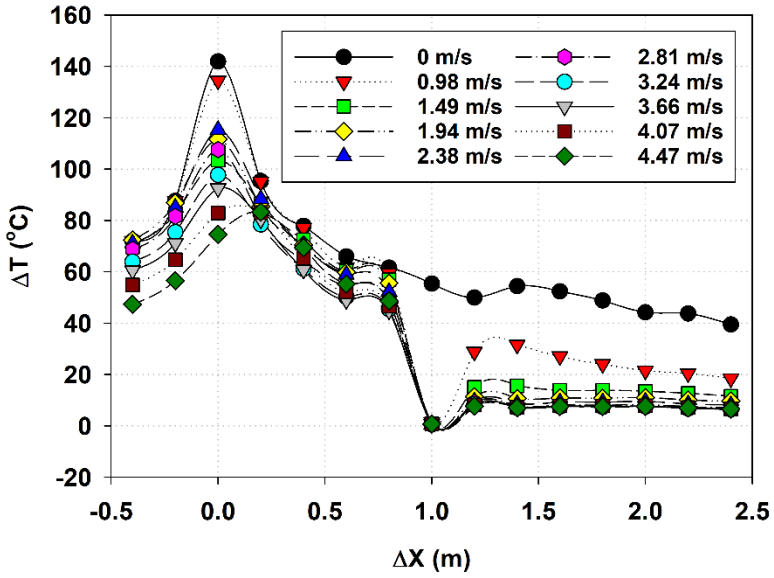

Figure 8. *Mean smoke temperature distribution along the longitudinal direction below the ceiling (Test 1-10: θ=0°, HRR=3.62 kW and W=3 cm).*

The influence of air curtain velocity on the temperature field within the compartment is visible. As demonstrated in [1] more back-flow with fresh air will move to the fire source as the air curtain velocity (or R) increases. This explains the decrease of temperature of upstream region close to the fire source for higher air curtain velocities (see Fig.5).

To be noted, this also illustrates the advantage of using a gas burner rather than a liquid pool fire for this study. Because the gas burner gives a constant HRR during the experiments without any influence from the air curtain.

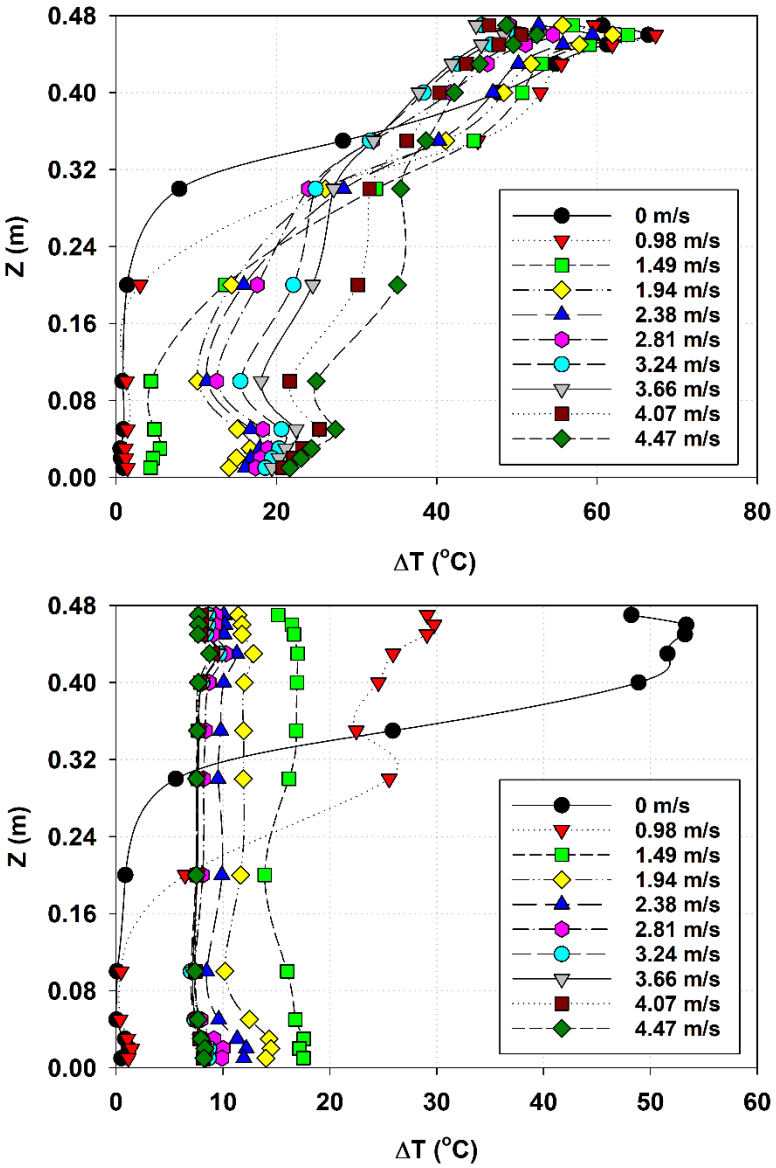

Figure 9. *Profiles of mean smoke temperature at the upstream (Top) and downstream (Bottom) of the air curtain (Test 1-10: θ=0°, HRR=3.62 kW and W=3 cm).*

Figure 9 shows the mean temperature profiles at the upstream (ΔX=0.8 m) and downstream (ΔX=1.2 m) of the air curtain for different air curtain velocities. For both of the upstream and downstream, the temperature profiles become flatter (more even distribution of temperature) as the air curtain velocity increases. Indeed, with increasing air curtain velocity, the flow field becomes more mixed.

However, the excess temperatures and temperature profiles in the downstream region are much lower and flatter than in the upstream regions, which demonstrates the sealing effect of the air curtain. This will be discussed in more details in the next section.

4.1.2 Influence of the air curtain width

The influence of the air curtain width is illustrated in Figure 10 and 11, taking Test 5, 24, 43 for example (Injection angle θ=0°, HRR=3.62 kW and air curtain velocity $V_j \approx 2.3$ m/s,). The mean smoke temperature distribution along the longitudinal direction at 1 cm below the ceiling is shown in Figure 10. Figure 11 shows the mean temperature profiles at the downstream (ΔX=1.2 m) of the air curtain for different curtain widths (Due to space limitations, we limit the discussion to the downstream area, i.e. the protection zone).

It can be seen that, with other parameters being constant, the longitudinal and vertical smoke temperature distributions downstream of the air curtain decrease as the width of the curtain increases. The sealing effectiveness is enhanced with the increase of nozzle width. This is due to the fact that with other parameters being constant, an increase in the nozzle width will result in increased air curtain momentum and mass flow. Specific quantitative analysis will be discussed in detail in the next section.

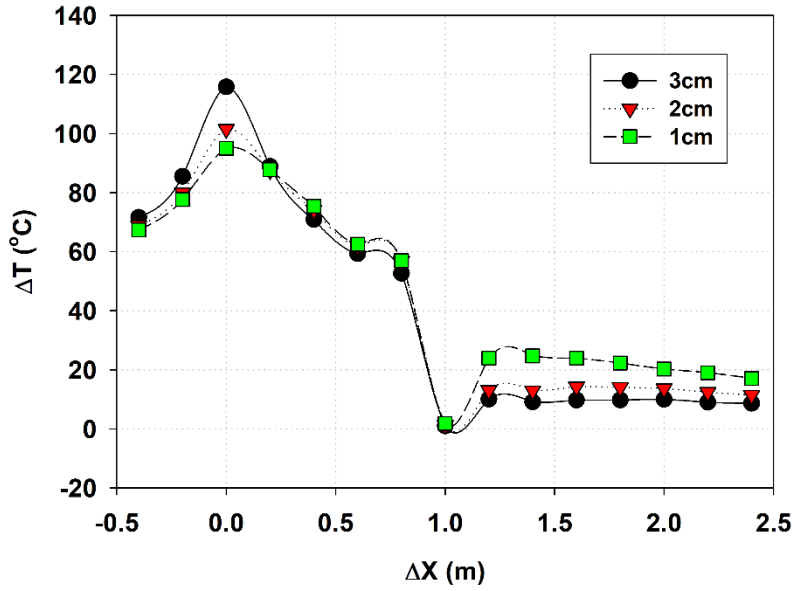

***Figure 10**. Mean smoke temperature distribution along the longitudinal direction below the ceiling (Test 5, 24, 43, θ=0°, HRR=3.62 kW and V_j≈2.3 m/s)*

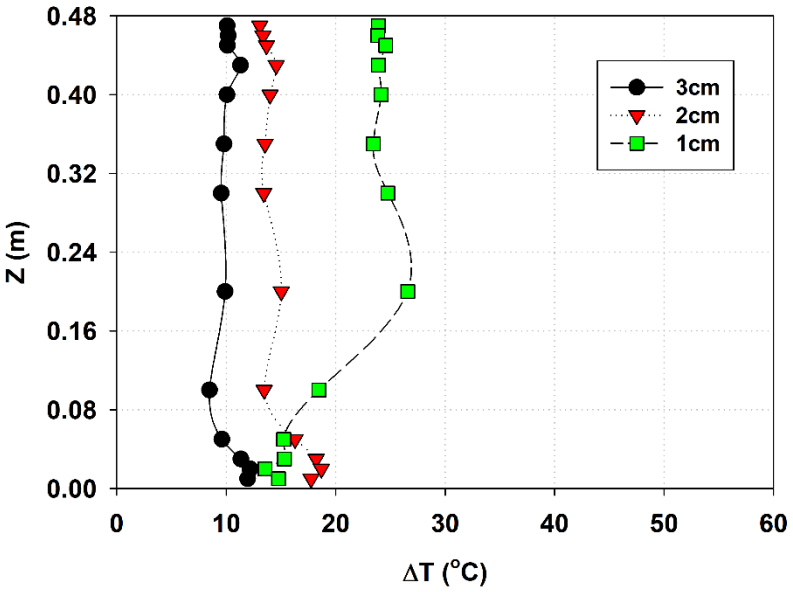

***Figure 11.** Profiles of mean smoke temperature at the downstream of the air curtain (Test 5, 24, 43, θ=0°, HRR=3.62 kW and V_j≈2.3 m/s)*

4.1.3 Influence of the air curtain angle

Then, the impact of air curtain injection angle is studied. The influence of different injection angles, i.e., θ=0° (Test 3, 5, 7, 9), θ=15° (Test 63, 65, 67, 69)

θ=30°(Test 73, 75, 77, 79) and θ=45° (Test 83, 85, 87, 89) is shown in Figures 12 and 13 for jet velocities of 1.49m/s, 2.38m/s, 3.24m/s and 4.07m/s resp. (with constant HRR = 3.62 kW and air curtain width W = 3 cm). As can be seen from Figs. 12 and 13, the effect of injection angle becomes more pronounced for higher jet velocity. In addition, the results from 0° and 15° are similar and close to each other. Both of these results are different from the similar resuts obtained at 30° and 45°. Overall, when the other parameters are fixed, for a jet angle of 30-45°, the overall longitudinal and vertical temperature distributions are lower than for 0-15°. Again, a specific quantitative analysis will be discussed in detail in the next section.

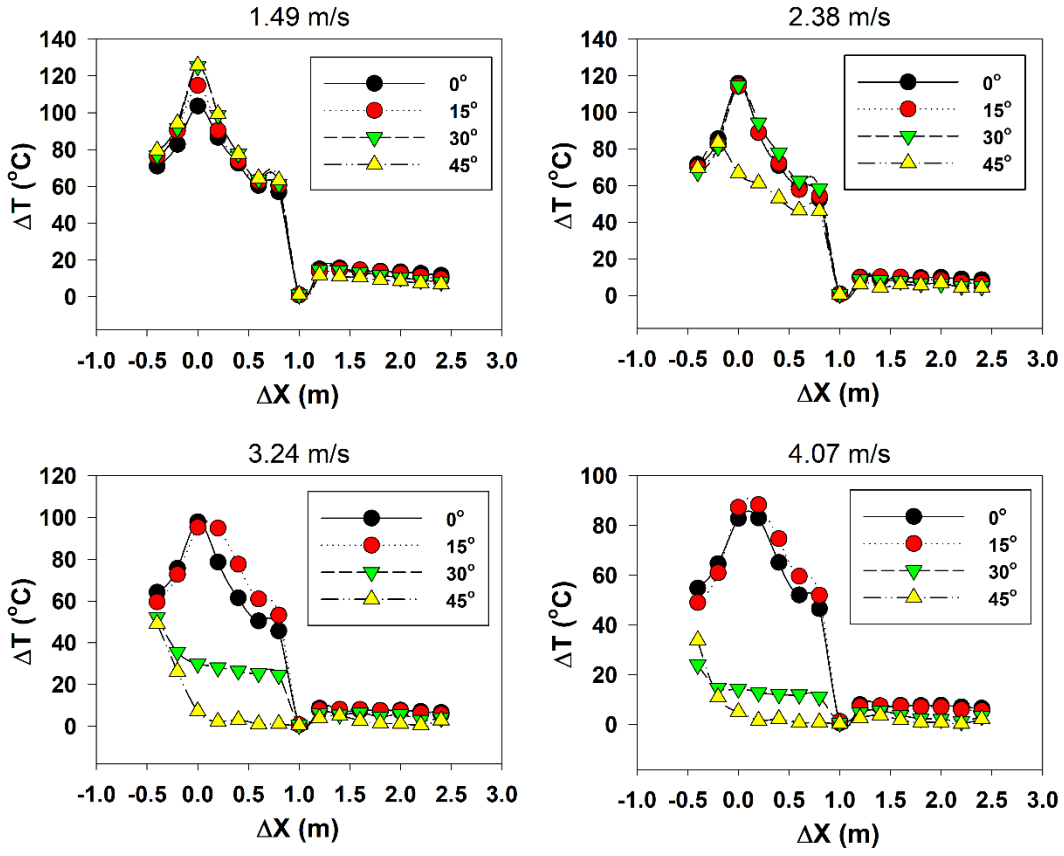

Figure 12. *Mean smoke temperature distribution along the longitudinal direction below the ceiling (HRR=3.62kW and W=3 cm): 1.49 m/s (Test 3, 63, 73, 83); 2.38 m/s (Test 5, 65, 75, 85); 3.24 m/s (Test 7, 67, 77, 87) and 4.07*

m/s (Test 9, 69, 79, 89)

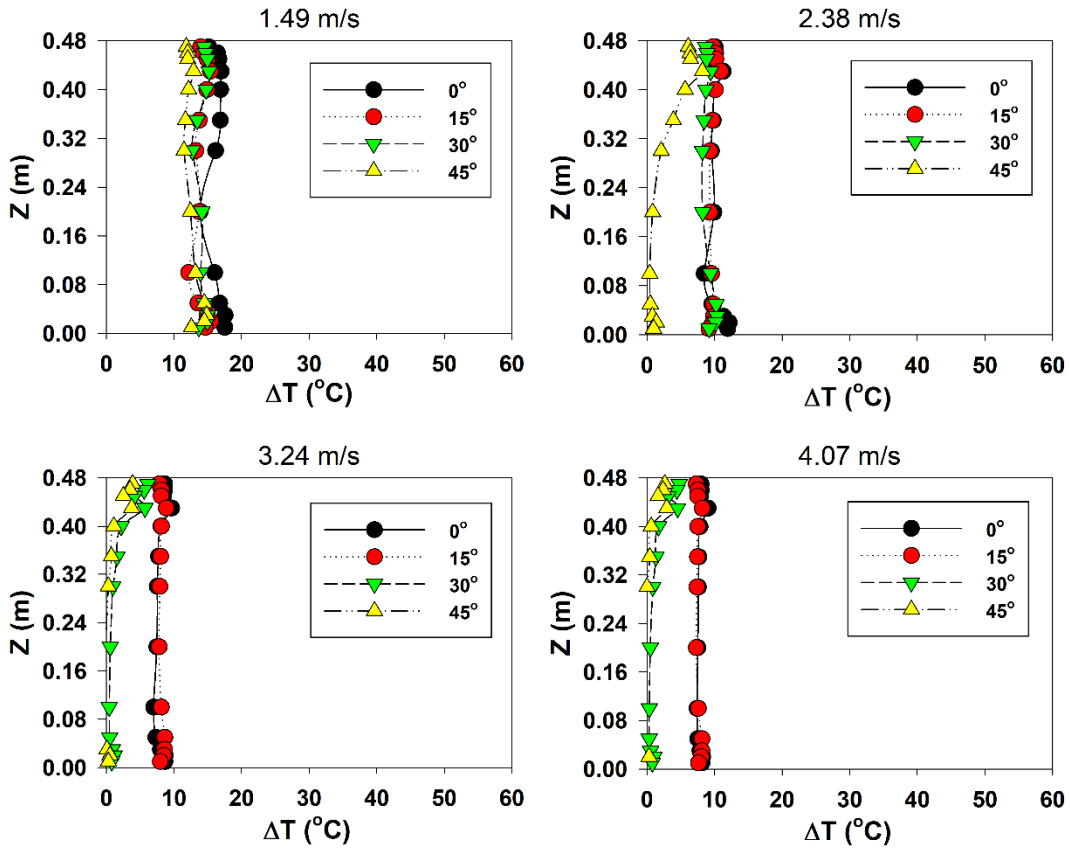

Figure 13. *Profiles of mean smoke temperature at the downstream of the air curtain (HRR=3.62kW and W=3 cm): 1.49 m/s (Test 3, 63, 73, 83); 2.38 m/s (Test 5, 65, 75, 85); 3.24 m/s (Test 7, 67, 77, 87) and 4.07 m/s (Test 9, 69, 79, 89)*

4.1.4 Influence of the fire HRR

Finally, the Influence of the fire HRR is studied. The impact of fire HRR is more intuitive. Fire HRR will affect the ceiling jet temperature and velocity distribution. According to the studies of Alpert [35] and Motevalli [36], the temperature and velocity of the ceiling jet are related to the fire HRR $\dot{Q}$, the tunnel height H and the distance r from the fire. Therefore, the momentum of the ceiling jet is a

function of $\dot{Q},\ H,\ r$, i.e., $\rho_s A_s {V_s}^2 = f(\dot{Q},\ H,\ r)$. Changing any of the fire HRR, the height of channel *H* and distance *r* from the fire can change the momentum of the ceiling jet. In order to facilitate the study, the ceiling jet momentum only changed by the fire HRRs in the present study.

For injection angle of 0°, air curtain width *W* = 3 cm and jet velocity of 0 m/s, 1.49 m/s, 2.38 m/s and 3.24 m/s, the mean smoke temperature distribution along the longitudinal direction at 1 cm below the ceiling is shown in Figure 14 for various HRRs. Figure 15 shows the mean temperature profiles at the downstream (ΔX=1.2 m) of the air curtain for different air curtain velocities (Due to space limitations, we limit the discussion to the downstream area, i.e. the protection zone).

As can be seen in Figures 14 and 15, when the air curtain velocity is 0 (i.e., the air curtain is not activated), the longitudinal temperature distribution and the vertical cross-section temperature distribution of the ceiling jet are higher for a larger fire HRR. This is consistent with the findings of Alpert [35] and Motevalli [36] that the temperature of the ceiling jet increases with increased HRR. The results are also similar for the other jet velocities. Specific quantitative analysis will be discussed in detail in the next section.

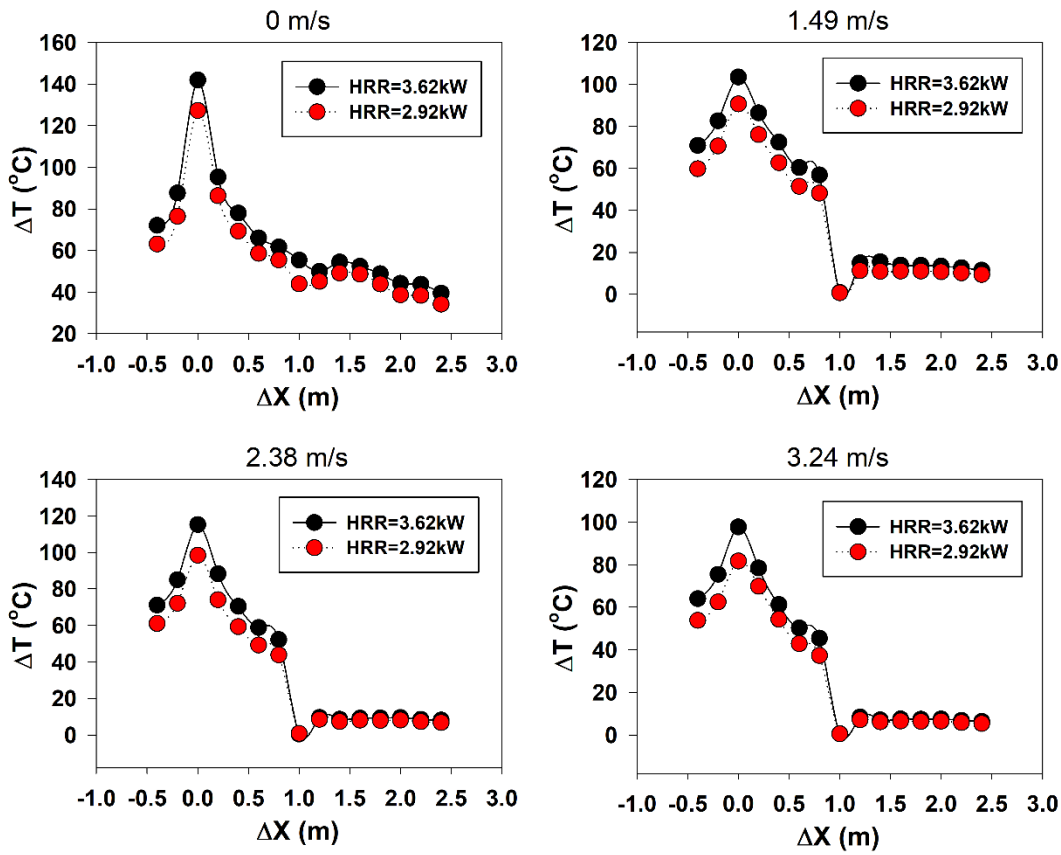

Figure 14. *Mean smoke temperature distribution along the longitudinal direction below the ceiling (Test 1, 3, 5 and 7 Vs Test 11, 13, 15 and 17, W=3 cm)*

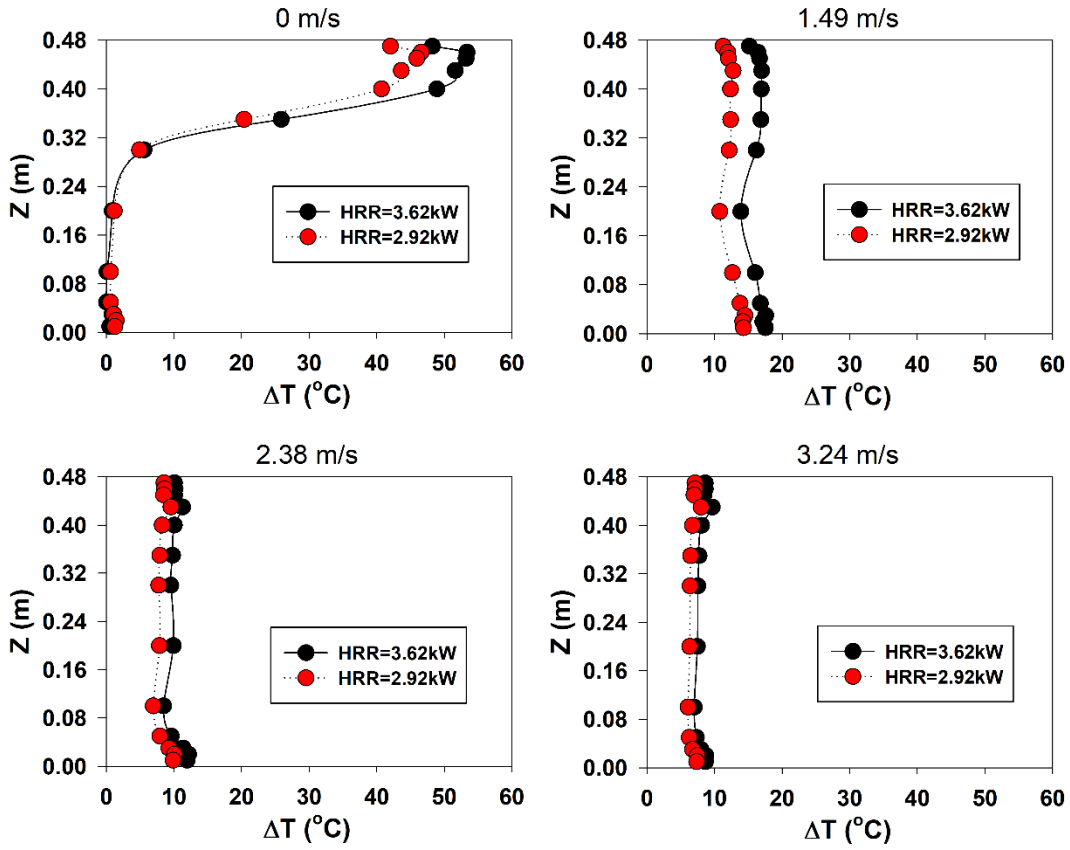

Figure 15. *Profiles of mean smoke temperature at the downstream of the air curtain (Test 1, 3, 5 and 7 Vs Test 11, 13, 15 and 17, W=3 cm)*

4.2 Sealing effectiveness E as a function of the momentum ratio R

4.2.1 Definition of the sealing effectiveness E

The sealing effect (performance) of an air curtain, i.e., its ability to reduce the heat and mass transfer, can be assessed in terms of (local) sealing effectiveness E_{local}. Due to the limited number of thermocouples, the sealing effectiveness E_{local} is defined here locally compared to the previous definition [1], in terms of the difference between the overall temperature rise, ΔT_{V_j}, obtained from integration over the height of the tunnel in the downstream region of the air curtain, and the reference value, $\Delta T_{V_j=0}$, when the air curtain is absent:

$$E_{local} = 1 - \frac{\Delta T_{V_j}}{\Delta T_{V_{j=0}}} \quad (3)$$

ΔT_{V_j} has been calculated as:

$$\Delta T_{V_j} = \frac{1}{Z}\int (T_{V_j}(z) - T_{amb})dz \quad (4)$$

where Z is the height of the tunnel over which the integrated temperature rise is calculated.

In addition, for the purpose of an easy comparison with the results displayed in [1], we define here the mean sealing effectiveness of the air curtain E_{mean} calculated as the average of the n local sealing effectiveness E_{local} as follow:

$$E_{mean} = \frac{1}{n}\sum E_{local} \quad (5)$$

4.2.2 Definition of the momentum ratio R

As mentioned above, the sealing effect of a vertical-downward air curtain is influenced by the air curtain velocity, slot width and fire HRR. The influence of the three variables could be integrated into a parameter called the momentum ratio R, defined as the ratio of the vertically downward air curtain momentum to the horizontal smoke layer momentum at the position of the air curtain [1].

$$R = \rho_j A_j {V_j}^2 / \rho_s A_s {V_s}^2 \quad (6)$$

If the air curtain is discharged with an angle, the momentum ratio R is then calculated based on the vertical downward component of the total air curtain momentum to the horizontal smoke layer momentum at the position of the air curtain.

$$R = \rho_j A_j {V_j}^2 cos\theta / \rho_s A_s {V_s}^2 \quad (7)$$

As mentioned, the sealing effect of an air curtain is influenced by the air curtain

and ceiling jet properties. The air curtain can be characterized by the air curtain momentum $\rho_j A_j V_j^2 cos\theta$, which includes all the parameters determining the strength of the air curtain flow (slot width, curtain velocity and injection angle). The ceiling jet can be characterized by the ceiling jet momentum $\rho_s A_s V_s^2$, which also includes all the parameters determining the strength of the ceiling jet ($\rho_s A_s V_s^2 = f(Q,\ H,\ r)$). Thus, the influence from different factors can be expressed as a dimensionless quantity—momentum ratio R for the sake of convenience.

4.2.3 Results in terms of E and R

Figure 16 shows the relationship between the local sealing effectiveness E_{local} at different distances from the fire and the momentum ratio R for air curtain with different widths. Each figure includes six profiles with combinations of two parameters, i.e., HRRs and different distances from the fire in the downstream region.

In each figure the profiles from different HRRs are self-similar and overlap with each other, which means that an equivalent sealing effect of an air curtain under different HRRs is achieved as long as the momentum ratio R is equalized.

Secondly, the local sealing effectiveness E_{local} varies with the location in the downstream region. Generally, a higher local sealing effectiveness E_{local} is obtained in the region closer to the air curtain. This is may be due to the impingement of the air curtain on the floor and thus entraining smoke further downstream.

Thirdly, the local sealing effectiveness E_{local} is also strongly influenced by the air curtain velocity (or momentum ratio R). Especially for the small values of R,

the temperature distribution at different locations is different. This is due to the uneven temperature distribution in the downstream region. The three profiles in the downstream region reach a plateau for high values of momentum ratio, R. However, high values of R are, in general, undesired because it can lead to additional oxygen supply to the fire seat, due to the impingement on the floor. This situation can be hazardous in case of under-ventilated fires. In each figure, local sealing effectiveness E_{local} in the downstream region reach a maximal value at around R ≈ 10. In other words, a momentum ratio of R ≈ 10 is recommended for the optimal sealing effect of a vertical downward air curtain. This is in line with [1].

Finally, by comparing the sub-figures of Fig. 16 in a column, one can observe that all profile shapes from different slot widths are similar. However, the local sealing effectiveness E_{local} in the downstream region is higher with wider slot width, which means, for the same value of momentum ratio R, a better sealing effect is achieved for a wider slot width. Another aspect is that for a constant momentum ratio R, less fresh air is injected as the width decreases (see Fig.3). In other words, a higher temperature is to be expected for smaller width, based on an energy balance.

More interesting, not only a lower local sealing effectiveness E_{local} is resulted for a narrower slot, but also an even worse situation can occur. In other words, a narrow slot with small value of width (e.g., W=1 cm) can deteriorate the sealing effect and even lead to more smoke being entrained to the downstream region (looking at the negative values of sealing effectiveness), which is the unfavourable situation that should be avoided. The influence of slot width will be investigated quantitatively in the next sub-section.

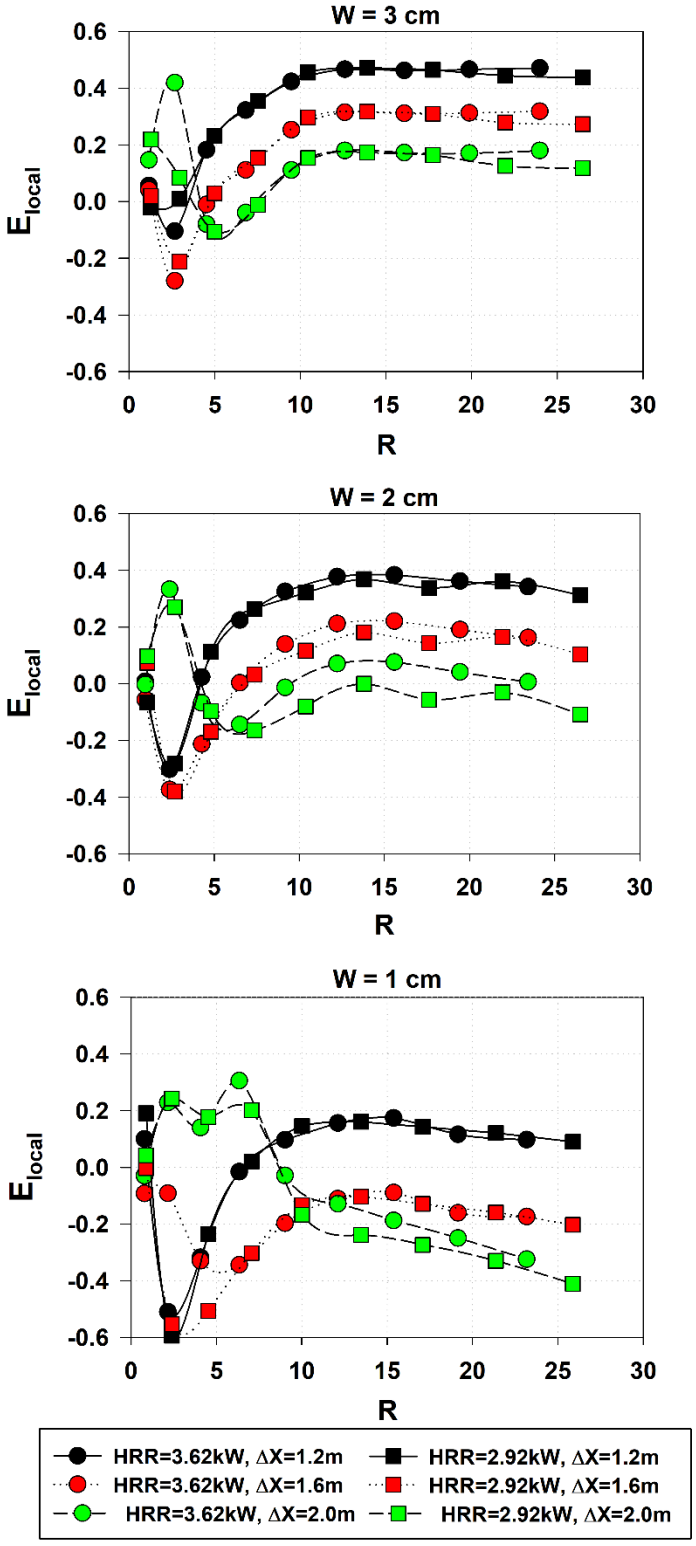

Figure 16. *Local sealing effectiveness* E_{local} *at different distances from the fire versus momentum ratio R for air curtain with different widths.*

So far, the discussion has been restricted to the case of vertical-downward air

curtain. As mentioned in Table 1(b), 3 other injection angles were investigated as well.

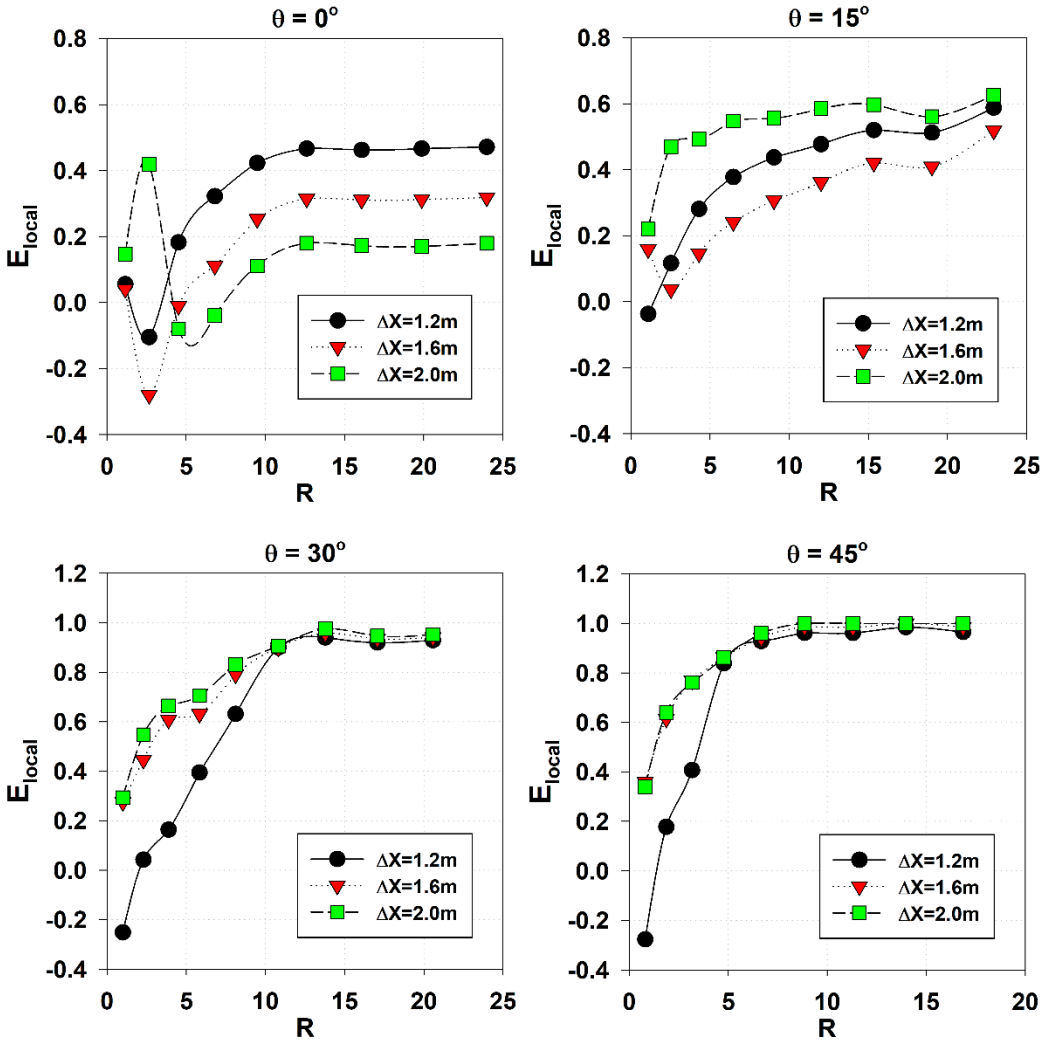

Figure 17. *Local sealing effectiveness* E_{local} *at different distances from the fire versus momentum ratio R for different injection angles.*

Figure 17 shows the relationship between the local sealing effectiveness E_{local}, at different distances from the fire, and the momentum ratio R for different injection angles. Similar to the vertical-downward air curtain, for non-vertical-downward air curtain with different injection angles, the maximum sealing effectiveness is also attained for R ≈ 10. However, R is calculated as the ratio

of the vertically-downward component of the total air curtain momentum to the horizontal smoke layer momentum at the position of the air curtain (see Eq. (7)). To be noted, the maximum sealing effectiveness increases as the injection angles increases. This is due to the increasing horizontal component of air curtain momentum as the injection angle increases from 0° to 45° (The angle θ is shown in Fig. 4). The influence of injection angle will be investigated quantitatively in next sub-section.

4.2.4 Maximum E

As presented in the previous sub-sections, when using air curtain for fire-induced smoke confinement in a tunnel configuration under different fire HRRs with different set-up of air curtains (jet velocity, slot width and injection angle), the non-dimensional parameter (momentum ratio) R ≈ 10 is recommended for a maximum sealing effectiveness. However, the attained value of maximum sealing effectiveness depends on the slot width and injection angle.

Figure 18 shows the influence of slot widths (a) and injection angles (b) on the mean sealing effectiveness E_{mean} where E_{mean} is calculated as the average of the local sealing effectiveness E_{local} at different cross sections (see Eq. (5)). Figure 18 (a) and (b) confirm the previous finding that the mean sealing effectiveness E_{mean} increases as the momentum ratio R increases, and a maximum sealing effectiveness is attained for R ≈ 10 for all cases with different slot widths and injection angles.

More importantly, as shown in Figure 18 (a), at a certain momentum ratio R, the mean sealing effectiveness increases as the slot width increases. This is may be due to the increase of air curtain mass flow rate for a wider slot width.

($R \sim f(W_j {V_j}^2)$, for $R = W_{j1}{V_{j1}}^2 = W_{j2}{V_{j2}}^2$, if $W_{j1} > W_{j2}$, then $V_{j1} < V_{j2}$ and $\frac{W_{j1}V_{j1}}{W_{j2}V_{j2}} = \frac{V_{j2}}{V_{j1}} > 1$). Therefore, for a certain momentum ratio R, the increase on mean sealing effectiveness for a wider slot width is mainly contributed from the stronger dilution effect due to the increase of air curtain mass flow rate. To characterize this effect, the (dimensionless parameter) slot shape factor AR is defined as the ratio of the slot width W divided by the slot length L, i.e., AR= W/L. This effect is not significant in increasing the performance of air curtain for smoke confinement. The net increase on mean sealing effectiveness is 20% when increasing the slot width from 1 cm to 2 cm. This value drops to 10% when increasing the slot width from 2 cm to 3 cm. Noted, a small-scale slot width of 1 cm – 3 cm corresponds to a full scale width of 10 cm - 30 cm, if taking a geometrical scale-up factor of 10.

Similarly, as shown in Figure 18 (b), for a given momentum ratio R, the mean sealing effectiveness increases as the injection angle increases. An abrupt net-increase on the mean sealing effectiveness (from 50% to 90%) is observed at increasing injection angle from 15 ^{o} to 30^{o}. With further increasing the injection angle from 30 ^{o} to 45^{o}, the net-increase on the mean sealing effectiveness is less than 10%. Thus, an optimal injection angle of 30 ^{o} can be recommended. Another important finding is that, based on the present experimental data, changing the injection angle has a more significant effect on the sealing effectiveness than varying the slot width under the existing investigated data range. Thus, the injection angle should be considered first in the engineering design process of the air curtain for smoke confinement.

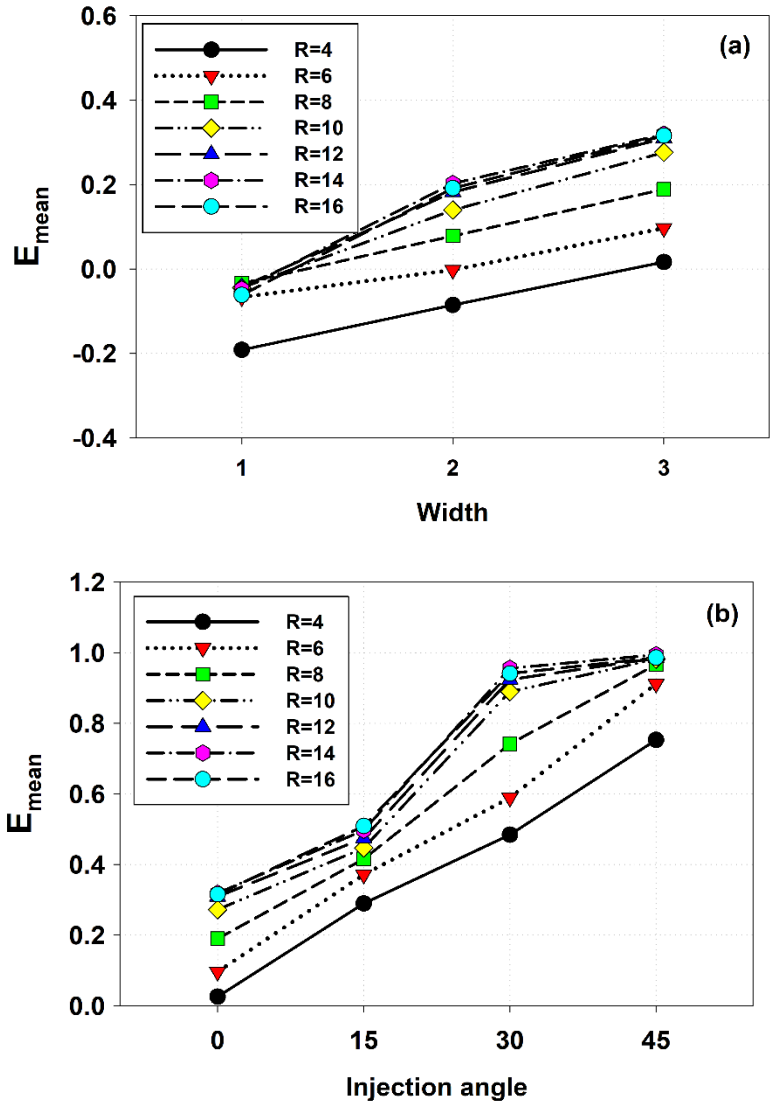

Figure 18. *Mean sealing effectiveness* E_{mean} *versus the slot widths (a) and injection angles (b).*

5. Conclusions

Experimental data have been presented for small scale fire tests in a tunnel configuration, under the effect of an air curtain for smoke blocking. A range of fire HRRs, air curtain discharge velocities, slot widths and injection angles have been considered. The main objective of this paper is to understand the effect of those parameters on the sealing effectiveness of the air curtain and to provide practical guidance on the engineering design of the air curtain for smoke

confinement.

Three important parameters that determine the performance of air curtains for smoke confinement are presented, i.e., (1) the dimensionless momentum ratio R that characterizes the relative force between the air curtain and the smoke motion (as ceiling jet), (2) the dimensionless shape factor AR (AR=W/L) that characterizes the dilution effect of the air curtain jet, and (3) the injection angle θ that characterizes the horizontal force of the air curtain.

The presented experimental data validated the finding that a momentum ratio of $R \approx 10$ is recommended for the optimum sealing effect of a vertical downward air curtain used for fire-induced smoke confinement in a tunnel configuration. For a non-vertical-downward air curtain with different injection angles, the maximum sealing effectiveness is also attained for $R \approx 10$, providing the vertically-downward component of the total air curtain momentum being used to calculate the momentum ratio R.

The air curtain sealing effectiveness increases with both the increase of slot width (shape factor AR) and injection angle (θ). A total increase of sealing effectiveness of 30% and 70% is found respectively with the increase of slot width from 1cm to 3cm and the increase of injection angle from 0^{o} to 45^{o}. The air curtain width has limited influence on the performance of the air curtain whilst the injection angle has a more significant influence on the sealing effectiveness of the air curtain under the existing investigated data range. An optimal injection angle of 30^{o} inclined to the fire source is recommended in the engineering design of the air curtain for smoke confinement for situations where the fire location can be pre-determined to be only at one side of an air curtain.

Acknowledgements

This research was supported by the State Scholarship Fund (Grant No. 201306050081), National Natural Science Foundation of China (Grant No. 51608076), Chongqing Science and Technology Commission (Grant No. cstc2016shmszx30016), Chongqing Construction Science and Technology Planning Project (Grant No. 2015-1-34), Fundamental Research Funds for the Central Universities (Grant No. 106112015CDJXY210008), graduate scientific research and innovation foundation of Chongqing, China (Grant No. CYB16006) and the 111Project, No. B13041.

Reference

1. Yu, L.-X., et al., *Simulations of Smoke Flow Fields in a Wind Tunnel Under the Effect of an Air Curtain for Smoke Confinement.* Fire Technology, 2016. **52**(6): p. 2007-2026.
2. McGrattan, K., et al., *Computational fluid dynamics modelling of fire.* International Journal of Computational Fluid Dynamics, 2012. **26**(6-8): p. 349-361.
3. McDermott, R. *FDS Release Notes*. 2017 20 Jan [cited 2017 30 Jun]; Available from: https://github.com/firemodels/fds/wiki/FDS-Release-Notes.
4. Alarie, Y., *Toxicity of fire smoke [Review].* Critical Reviews in Toxicology, 2002. **32**(4): p. 259-289.
5. Fan, C.G., et al., *Experimental study of air entrainment mode with natural ventilation using shafts in road tunnel fires.* International Journal of Heat and Mass Transfer, 2013. **56**(1): p. 750-757.
6. Guyonnaud, L., et al., *Design of air curtains used for area confinement in tunnels.* Experiments in Fluids, 2000. **28**(4): p. 377-384.
7. Sakurai, H., et al., *Researches on air shutter for fire defence.* Fire Safety

Journal, 1980. **2**(1): p. 9-16.

8. Hu, L.H., et al., *Confinement of fire-induced smoke and carbon monoxide transportation by air curtain in channels.* Journal of Hazardous Materials, 2008. **156**(1–3): p. 327-334.
9. Ji, J., et al. *Critical Conditions for Fire-Induced Smoke Confinement by Air Curtain in Long Channels*. in *ASME 2009 Heat Transfer Summer Conference collocated with the InterPACK09 and 3rd Energy Sustainability Conferences*. 2009. American Society of Mechanical Engineers.
10. Krajewski, G. and W. Węgrzyński, *Air curtain as a barrier for smoke in case of fire: Numerical modelling.* Bulletin of the Polish Academy of Sciences Technical Sciences, 2015. **63**(1): p. 145-153.
11. Yu, L.-X., et al., *Analysis of FDS 6 Simulation Results for Planar Air Curtain Related Flows from Straight Rectangular Ducts.* Fire Technology, 2017.
12. Yu, L.-X., et al., *Assessment of Numerical Simulation Capabilities of the Fire Dynamics Simulator (FDS 6) for Planar Air Curtain Flows.* Fire Technology, 2018.
13. Luo, N., et al., *An experiment and simulation of smoke confinement utilizing an air curtain.* Safety Science, 2013. **59**(0): p. 10-18.
14. Gao, R., et al., *Study of a proposed tunnel evacuation passageway formed by opposite-double air curtain ventilation.* Safety Science, 2012. **50**(7): p. 1549-1557.
15. Altinakar, M. and A. Weatherill. *Use of an inclined air curtain for preventing smoke propagation in a tunnel during fire emergency*. in *Proceedings of the fourth international conference on safety in road and rail tunnels, Held Madrid, Spain, 2-6 April*. 2001.
16. Nyman, H. and H. Ingason, *Air curtains can protect against the spread of fire gases in underground railways.* SP Rapport, 2014: p. 06.
17. Costa, J., L. Oliveira, and M. Silva, *Energy savings by aerodynamic*

sealing with a downward-blowing plane air curtain—a numerical approach. Energy and Buildings, 2006. **38**(10): p. 1182-1193.

18. Cao, G., K. Sirén, and S. Kilpeläinen, *Modelling and experimental study of performance of the protected occupied zone ventilation.* Energy and Buildings, 2014. **68, Part A**(0): p. 515-531.
19. Ciocănea, A. and A. Dragomirescu, *Modular ventilation with twin air curtains for reducing dispersed pollution.* Tunnelling and Underground Space Technology, 2013. **37**(0): p. 180-198.
20. Hayes, F. and W. Stoecker, *Design data for air curtains.* Ashrae Transactions, 1969. **75**(2): p. 168-180.
21. Hayes, F. and W. Stoecker, *Heat transfer characteristics of the air curtain.* ASHRAE Transactions, 1969. **75**(2): p. 153-167.
22. McGrattan, K., et al., *Fire Dynamics Simulator, User's Guide*. Sixth ed. NIST Special Publication 1019. 2013: National Institute of Standards and Technology, Gaithersburg, Maryland, USA, and VTT Technical Research Centre of Finland, Espoo, Finland.
23. Merci, B. and P. Vandevelde, *Experimental study of natural roof ventilation in full-scale enclosure fire tests in a small compartment.* Fire Safety Journal, 2007. **42**(8): p. 523-535.
24. Hu, L.H., et al., *An experimental investigation and correlation on buoyant gas temperature below ceiling in a slopping tunnel fire.* Applied Thermal Engineering, 2013. **51**(1–2): p. 246-254.
25. Gao, Z., et al., *Experimental investigation on transverse ceiling flame length and temperature distribution of sidewall confined tunnel fire.* Fire Safety Journal, 2017. **91**: p. 371-379.
26. Yunus, A.C. and J.M. Cimbala, *Fluid mechanics: fundamentals and applications.* International Edition, McGraw Hill Publication, 2006: p. 185-201.
27. Merci, B. and T. Beji, *Fluid Mechanics Aspects of Fire and Smoke Dynamics in Enclosures*. 2016: CRC Press.

28. Khan, M.M., A. Tewarson, and M. Chaos, *Combustion characteristics of materials and generation of fire products*, in *SFPE Handbook of Fire Protection Engineering*. 2016, Springer. p. 1143-1232.
29. Brzezinska, D. and A.S. Markowski, *Experimental investigation and CFD modelling of the internal car park environment in case of accidental LPG release.* Process Safety and Environmental Protection.
30. Yu, L.-X., et al., *Assessment of numerical simulation capabilities of the Fire Dynamics Simulator (FDS 6) for planar air curtain flows.* Fire Technology (Under review), 2017.
31. McGrattan, K. and B. Toman, *Quantifying the predictive uncertainty of complex numerical models.* Metrologia, 2011. **48**(3): p. 173.
32. McGrattan, K.B., H.R. Baum, and R.G. Rehm, *Large eddy simulations of smoke movement.* Fire Safety Journal, 1998. **30**(2): p. 161-178.
33. Fan, C.G., et al., *Experimental study on transverse smoke temperature distribution in road tunnel fires.* Tunnelling and Underground Space Technology, 2013. **37**(0): p. 89-95.
34. Fan, C.G., et al., *An experimental study of temperature and heat flux in a channel with an asymmetric thermal plume.* Applied Thermal Engineering, 2017. **113**: p. 1128-1136.
35. Alpert, R.L., *Turbulent Ceiling-Jet Induced by Large-Scale Fires.* Combustion Science and Technology, 1975. **11**(5-6): p. 197-213.
36. Motevalli, V. and C.H. Marks, *Characterizing the unconfined ceiling jet under steady-state conditions: a reassessment.* Fire Safety Science, 1991. **3**: p. 301-312.